Available online at www.sciencedirect.com
ScienceDirect
Trans. Nonferrous Met. Soc. China 34(2024) 833−845
Transactions of Nonferrous Metals Society of China
www.tnmsc.cn

Effect of extrusion ratio on microstructure, texture, and mechanical properties of dual-phase Mg−8Li−6Zn−2Gd alloy

Yue-hua SUN[1,2], Fan ZHANG[2], Bin YANG[2], Jian REN[1,2], Guang-sheng SONG[1,2]

1. Key Laboratory of Green Fabrication and Surface Technology of Advanced Metal Materials, Ministry of Education, Anhui University of Technology, Maanshan 243002, China;
2. School of Materials Science and Engineering, Anhui University of Technology, Maanshan 243002, China

Received 9 October 2022; accepted 30 June 2023

Abstract: The microstructure observation, macrotexture analysis, and tensile test were conducted to investigate the effect of extrusion ratio on the microstructure, texture, and mechanical properties of Mg−8Li−6Zn−2Gd alloy. The results show that the as-homogenized Mg−8Li−6Zn−2Gd alloy consists of α-Mg, β-Li, MgLiZn, *I*-phase, and *W*-phase. After hot extrusion, eutectic *I*-phase is broken into fine particles, while *W*-phase maintains massive shape. Both α-Mg and β-Li matrices undergo dynamic recrystallization (DRX), and their grains gradually refine with increasing extrusion ratio. For α-Mg matrix, the weakening of basal texture and the strengthening of prismatic texture after hot extrusion are due to the activation of non-basal slip. For β-Li matrix, the appearance of obvious α and γ fiber textures after hot extrusion is associated with the dynamic recovery (DRV) and DRX. The tensile strength and elongation of the alloy are simultaneously improved by hot extrusion, and the best comprehensive mechanical properties are achieved when extrusion ratio is 16:1.

Key words: Mg−Li alloy; icosahedral quasicrystal phase; extrusion ratio; dynamic recrystallization; macrotexture; mechanical properties

1 Introduction

With the rapid development of aerospace industry and the intensification of energy shortage, the demand for lightweight structural materials in various industrial fields is becoming increasingly urgent. Mg−Li alloy is the lightest metal structural material with a density of 1.25−1.65 g/cm^3, and it is 1/4−1/3 lighter than common Mg alloy and 1/3−1/2 lighter than Al alloy, exhibiting a great development potential in lightweight, energy conservation, and emission reduction [1]. Moreover, Mg−Li alloy has high specific strength, excellent damping, weak anisotropy, and incomparable plastic deformation ability, showing a good application prospect in the fields of aerospace, military, and 3C industry [2]. However, compared with Al alloy, Ti alloy, and common Mg alloy, the low strength of Mg−Li alloy intensely restricts its wide application.

Alloying, as an effective way to enhance the mechanical properties of alloy, mainly realizes alloy strengthening by the solid solution of alloying elements in the matrix and the formation of second phases. Previous researches have revealed that Zn and several rare earth (RE) elements (such as Y, Gd, Er, and Nd) are simultaneously added into Mg alloy to form Mg−Zn−RE ternary phases, such as *W*-phase ($Mg_3Zn_3RE_2$, face-centered cubic structure), *I*-phase (Mg_3Zn_6RE, icosahedral quasi-crystal structure), and LPSO phase ($Mg_{12}ZnRE$, long-period stacking ordered structure), and the precipitation of these phases depends on the Zn/RE ratio [3−5]. Among them, *I*-phase has special

Corresponding author: Jian REN, Tel: +86-18321736726, E-mail: renjianahut@126.com
DOI: 10.1016/S1003-6326(23)66437-4

symmetry and maintains good coherent orientation relationship with α-Mg matrix, which effectively hinders the dislocation movement and shows a good room-temperature strengthening effect [6]. Moreover, *I*-phase has excellent thermal stability below 440 °C and thus exhibits a good high- temperature strengthening effect [6]. Recently, it has been reported that adding Zn and several RE elements (such as Y and Gd) into Mg−Li alloy enables the introduction of *I*-phase which can significantly improve the mechanical properties and corrosion resistance of the alloy [7−13]. Furthermore, the formation of *I*-phase remains largely unaffected by variation in the Li content. XU et al [8−10] introduced *I*-phase into Mg−6Li and Mg−8Li alloys by adding Zn and Y with a Zn/Y mass ratio higher than 5, and the results showed that the formation of *I*-phase could suppress the Li diffusion from β-Li to α-Mg and improve the thermal stability of β-Li, which could in turn effectively enhance the alloy strength at room and elevated temperatures. LI et al [11,12] introduced *I*-phase into Mg−4Li and Mg−14Li alloys by adding 6 wt.% Zn and 1 wt.% Y, and the results revealed that the formation of *I*-phase could weaken the grain texture and increase the tensile strength of as-extruded Mg−4Li and Mg−14Li alloys from 163 to 240 MPa and from 111 to 168 MPa, respectively. ZHANG et al [13] introduced *I*-phase into Mg−9Li alloy by adding Zn and Gd with a Zn/Gd mass ratio of 3, and the results illustrated that the highest strength of 230.9 MPa was achieved in as-extruded Mg−9Li−9Zn−3Y alloy and the improvement in tensile strength was mainly attributed to the existence of broken *I*-phase and the grain refinement. However, the literature on the *I*-phase reinforced Mg−Li alloy is still very limited.

Hot extrusion is a most common deformation method in the production of Mg alloys. Its stress state is three-dimensional compressive stress, which can effectively refine alloy grains, improve strength, and maximize the plasticity of alloy. This is particularly important for Mg alloys with poor plastic deformation capability. Extrusion ratio is a parameter that measures the amount of deformation during the hot extrusion process, and its selection directly determines the final structure and performance of products. If extrusion ratio is too large, the extrusion process may be blocked due to excessive extrusion pressure, which may prevent the extrusion process from proceeding normally and even damage the mold. If extrusion ratio is too small, it is not conducive to obtaining products with uniform structure and performance. Therefore, an appropriate extrusion ratio is crucial in ensuring uniform microstructure and alloy performance. However, the suitable extrusion ratio for *I*-phase reinforced dual-phase Mg−Li alloy needs to be verified.

Herein, Mg−8Li−6Zn−2Gd alloy was prepared to introduce *I*-phase, and the effect of extrusion ratio on the microstructure, texture, and mechanical properties of the alloy was investigated to explore the appropriate extrusion ratio for obtaining the optimal mechanical properties.

2 Experimental

The alloy (Mg−8Li−6Zn−2Gd) used in this work was prepared by melting pure Mg ingots (>99.99 wt.%), pure Li particles (>99.9 wt.%), pure Zn ingots (>99.99 wt.%), and Mg−Gd (30 wt.%) master alloy in a vacuum induction furnace under the protection of pure argon atmosphere. After mixing and holding at 750 °C for 10 min, the melt was poured into the preheated stainless steel container with a diameter of 80 mm and naturally cooled to room temperature. The obtained ingots were homogenized at 300 °C for 12 h, followed by hot extrusion at 260 °C with extrusion ratios of 10:1, 16:1, and 23:1 to get cylindrical bars, respectively.

The chemical composition of alloy was determined by an inductively coupled plasma optical emission spectroscope (ICP-OES), and the obtained results are listed in Table 1. Phase composition was obtained with a D/Max 2500 X-ray diffraction (XRD) using monochromatic Cu K_α radiation, and the scan ranged at 2θ values from 15° to 80° with a constant scan rate of 8 (°)/min and a step size of 0.02°. The microstructure was observed with an optical microscope (OM, XJP−6A), an electron probe microanalyzer (EPMA, JXA−8230), and a scanning electron microscope (SEM, Quanta−200) equipped with an energy dispersive X-ray spectroscope (EDS). The specimens for OM observation were mechanically polished and then etched with a metallographic etchant prepared with 1 g oxalic acid, 1 mL acetic acid, 1 mL nitric acid, and 200 mL deionized water. Texture was analyzed by an X-ray diffractometer

(D8 discover), and the specimens for texture analysis were mechanically polished and then etched with the metallographic etchant for 4−6 s to remove surface residual stress. Tensile tests were conducted with an electronic universal testing machine (MTS−858) at a displacement rate of 1 mm/min. The tensile specimens were machined from the as-extruded bars along the extrusion direction, and their dimensions were determined according to the National Standard GB/T 228.1—2010, with a diameter of 6 mm and a gauge length of 30 mm.

Table 1 Chemical composition of Mg−8Li−6Zn−2Gd alloy (wt.%)

Li	Zn	Gd	Mg
8.02	5.98	1.85	Bal.

3 Results and discussion

3.1 Microstructure

Figure 1 shows the XRD patterns of as-homogenized and as-extruded Mg−8Li−6Zn−2Gd alloys. It can be clearly seen that as-homogenized Mg−8Li−6Zn−2Gd alloy is composed of α-Mg, β-Li, MgLiZn (face-centered cubic structure), *W*-phase (face-centered cubic structure), and *I*-phase (icosahedral quasicrystal structure). The coexistence of *W*-phase and *I*-phase has also been observed in previous researches on Mg−Li−Zn−Y alloys [8,9] and Mg−Li−Zn−Gd alloys [13]. After hot extrusion, the phase composition of the alloy does not change, but some diffraction peaks of *W*-phase and *I*-phase are slightly more obvious.

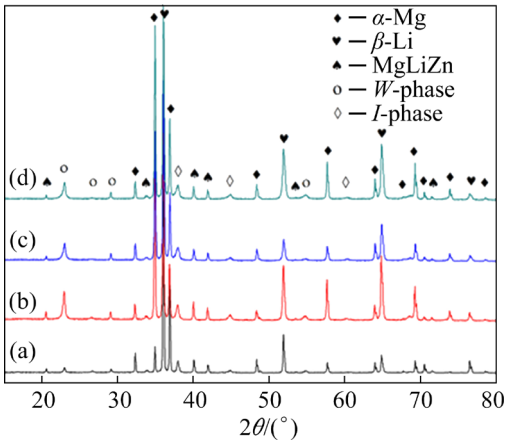

Fig. 1 XRD patterns of as-homogenized (a) and as-extruded (b−d) Mg−8Li−6Zn−2Gd alloys with different extrusion ratios of 10:1 (b), 16:1 (c), and 23:1 (d)

Figure 2 shows the SEM micrographs of as-homogenized Mg−8Li−6Zn−2Gd alloy observed at different magnifications. From low magnification microstructure shown in Fig. 2(a), the as-homogenized Mg−8Li−6Zn−2Gd alloy is a typical dual-phase Mg−Li alloy composed of α-Mg matrix and β-Li matrix, which is consistent with the XRD results shown in Fig. 1. Light-gray α-Mg phase exists in the alloy in block and long-strip shapes, and dark-gray β-Li phase fills in the space between α-Mg phases. Besides, a large number of spherical particles are distributed in β-Li matrix and along the α-Mg/β-Li phase interface, and some fishbone-like eutectic structures and massive phases can be observed in α-Mg matrix as well as along the α-Mg/β-Li phase interface.

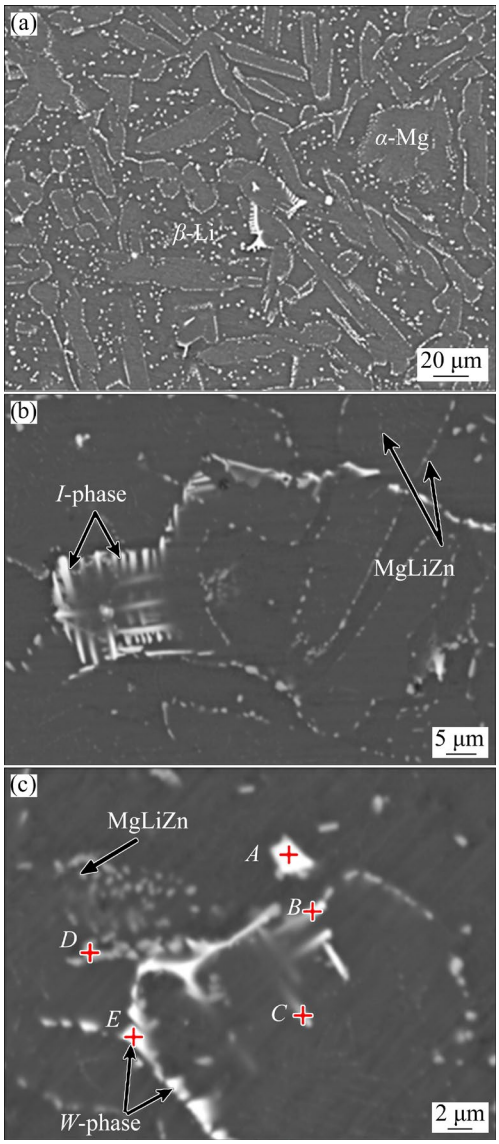

Fig. 2 SEM micrographs of as-homogenized Mg−8Li−6Zn−2Gd alloy

From the high magnification microstructure shown in Figs. 2(b) and (c), the contrast of eutectic phase and massive phase is brighter than that of spherical particle phase, which means that the eutectic phase and massive phase contain elements with larger atomic number. In order to identify these second phases, EDS analysis was carried out and the results are listed in Table 2. As shown in Fig. 2(c), the massive phases marked by Point *A* and Point *E* mainly contain Mg, Zn, and Gd, and their Zn/Gd molar ratios are close to 1.5. The eutectic phases marked by Point *B* and Point *C* mainly contain Mg, Zn, and Gd, and their Zn/Gd molar ratios are close to 6. The spherical granular phase marked by Point *D* mainly contains Mg and Zn but almost no Gd. Combined with the XRD results and previous studies [10,14], the massive phase, eutectic phase, and spherical granular phase are confirmed to be *W*-phase ($Mg_3Zn_3Gd_2$), *I*-phase (Mg_3Zn_6Gd), and MgLiZn phase, respectively. Therefore, the brighter contrast of massive phase and eutectic phase is attributed to the existence of Gd element with a large atomic number (Z=64). As previously reported in Refs. [7,14], *I*-phase and *W*-phase can be distinguished by their unique morphologies in as-cast microstructure. That is, the dendritic precipitate in fishbone-like eutectic structure is *I*-phase, and the massive precipitate distributed along the phase interface or at the edge of *I*-phase is *W*-phase [15,16]. The MgLiZn phase is observed in the previous investigation of Mg−Li−Zn−RE alloys, except for the granular MgLiZn phase distributed in *β*-Li matrix and *α*-Mg/*β*-Li phase interface, and the lamellar MgLiZn phase is found in *α*-Mg matrix [8,10]. Herein, a small amount of lamellar MgLiZn phase is distributed in *α*-Mg matrix, but it is not very obvious.

Table 2 EDS results of second phases marked by red crosses in Fig. 2 (at.%)

Point in Fig. 2(c)	Mg	Zn	Gd
A	88.67	6.88	4.45
B	86.85	11.32	1.83
C	89.21	9.28	1.51
D	82.44	17.55	0.01
E	90.71	5.53	3.76

Figure 3 displays the EPMA images of as-homogenized Mg−8Li−6Zn−2Gd alloy. Clearly, the granular MgLiZn phase with dark contrast mainly contains Mg and Zn, and both the fishbone-like eutectic *I*-phase and massive *W*-phase with bright contrast mainly contain Mg, Zn, and Gd, which are consistent with the EDS results in Fig. 2. In addition, some massive *W*-phase can be found at

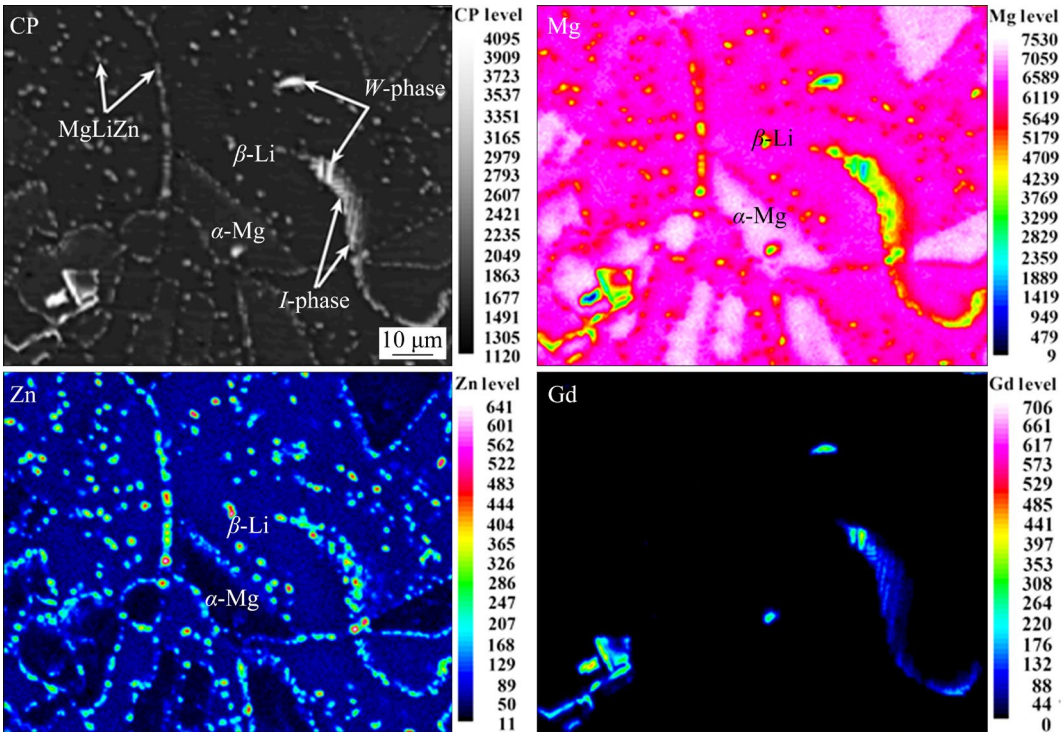

Fig. 3 EPMA images of as-homogenized Mg−8Li−6Zn−2Gd alloy

the edge of eutectic *I*-phase, and this *W*-phase contains more Gd element and shows brighter contrast compared with *I*-phase. As previously reported [17], *I*-phase can be precipitated directly from the melt through eutectic reaction ($L \rightarrow \alpha$-Mg + *I*-phase), or obtained from the reaction of liquid phase and *W*-phase through *W*-phase transformation reaction (L + *W*-phase → α-Mg + *I*-phase). Therefore, it can be observed that some *W*-phase and *I*-phase are next to each other. Zn element is mainly distributed in β-Li matrix because the solid solubility of Zn in β-Li matrix (12.5 wt.%) is higher than that of Zn in α-Mg matrix (6.2 wt.%). The added Zn element partially forms MgLiZn phase, *I*-phase, and *W*-phase, and the rest is mainly solid dissolved in β-Li matrix.

Figure 4 shows the SEM micrographs of as-extruded Mg−8Li−6Zn−2Gd alloy with different extrusion ratios. After hot extrusion, both α-Mg and β-Li phases are elongated along the extrusion

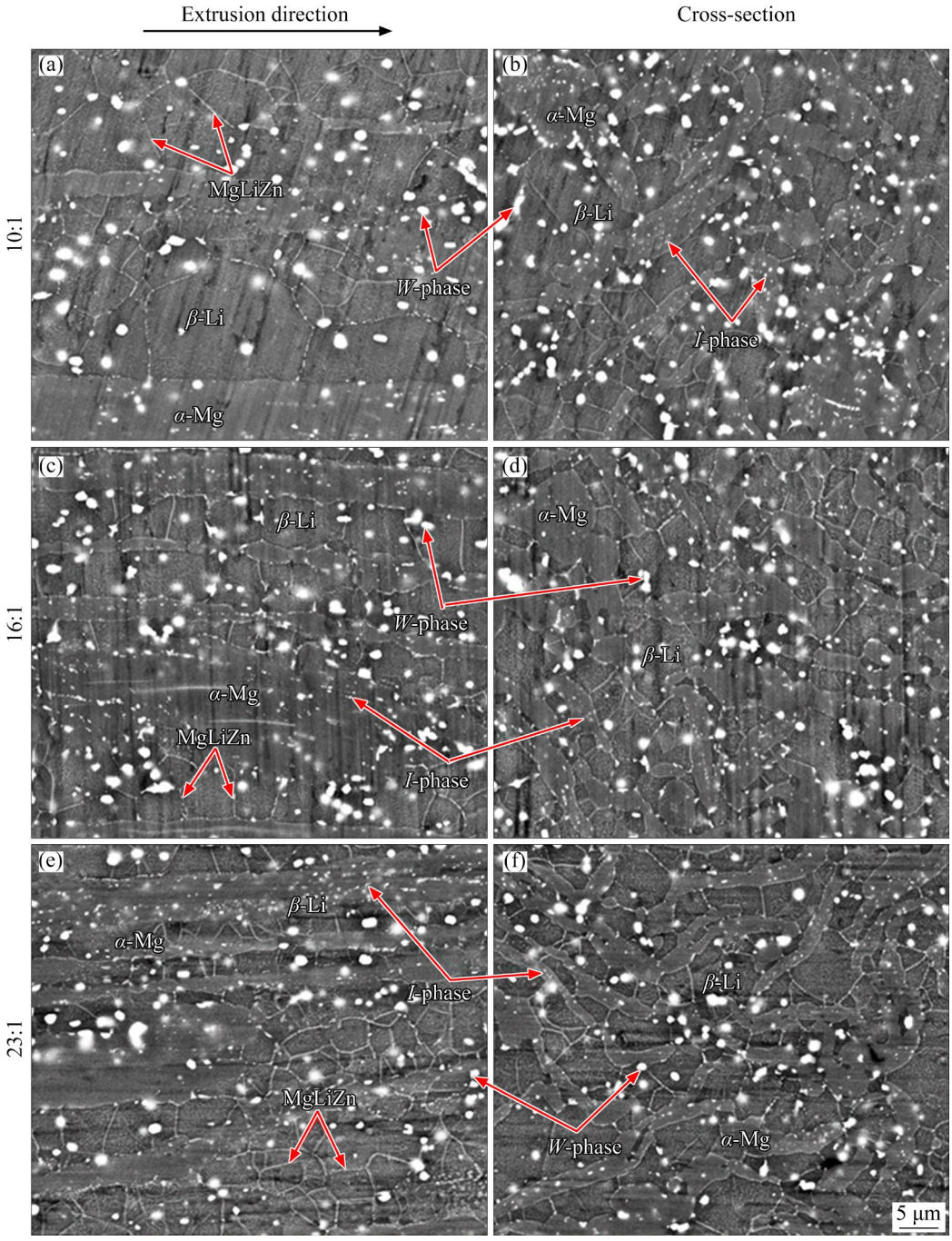

Fig. 4 SEM images of as-extruded Mg−8Li−6Zn−2Gd alloy with different extrusion ratios of 10:1 (a, b), 16:1 (c, d), 23:1 (e, f)

direction and distributed as banded structure, and the banded structure becomes slender with the increase of extrusion ratio. The granular MgLiZn phase maintains its original morphology, the fishbone-like eutectic *I*-phase is broken into fine particles, and the massive *W*-phase is dispersed more evenly after hot extrusion. Moreover, a kind of threadlike phase can also be observed along the grain boundaries of *β*-Li matrix in the as-extruded alloys, and its morphology is similar to that of the threadlike $MgLi_2Al$ phase in the as-extruded Mg−Li−Al−Zn alloy [18,19]. It may be MgLiZn phase precipitated from *β*-Li matrix during hot extrusion [20]. Therefore, it is evident that *β*-Li matrix undergoes DRX, and the grains are refined remarkably. ImageJ software is used to measure the average grain size of *β*-Li matrix. As the extrusion ratio increases from 10:1 to 16:1, and 23:1, the average grain sizes of *β*-Li matrix decrease gradually and they are 6.35, 5.47, and 3.91 μm, respectively.

Figure 5 illustrates the OM images of the as-homogenized and as-extruded Mg−8Li−6Zn−2Gd alloys. In order to observe the grains of *α*-Mg matrix more clearly, the corrosion time is accordingly prolonged, leading to the fuzzy grain boundaries of *β*-Li matrix. It is mainly due to the difference of corrosion resistance between *α*-Mg matrix and *β*-Li matrix. After hot extrusion, the *α*-Mg matrix changes from random distribution to strip distribution along extrusion direction, and the spacing between strip *α*-Mg matrix decreases with increasing the extrusion ratio. When the extrusion ratio is 10:1, some fine equiaxed grains and elongated coarse grains can be found in *α*-Mg matrix, indicating that incomplete DRX occurs in *α*-Mg matrix during extrusion. With the increase of extrusion ratio, the number of fine recrystallized grains gradually increases, while the number of elongated coarse grains gradually decreases. However, when the extrusion ratio increases to 23:1, there are still a few coarse deformed grains, which indicates that the DRX of *α*-Mg matrix is incomplete.

3.2 Texture

Figure 6 displays the orientation distribution function (ODF) sections at φ_2=0° and φ_2=30° of *α*-Mg matrix for as-homogenized and as-extruded Mg−8Li−6Zn−2Gd alloys. In the as-homogenized alloy, the texture of *α*-Mg matrix is formed mainly by $\{0001\}\langle 2\bar{1}\bar{1}0\rangle$ basal, $\{11\bar{2}0\}\langle 0001\rangle$ and $\{10\bar{1}0\}\langle 6\bar{3}\bar{3}10\rangle$ prismatic texture components, and the intensities of these texture components are

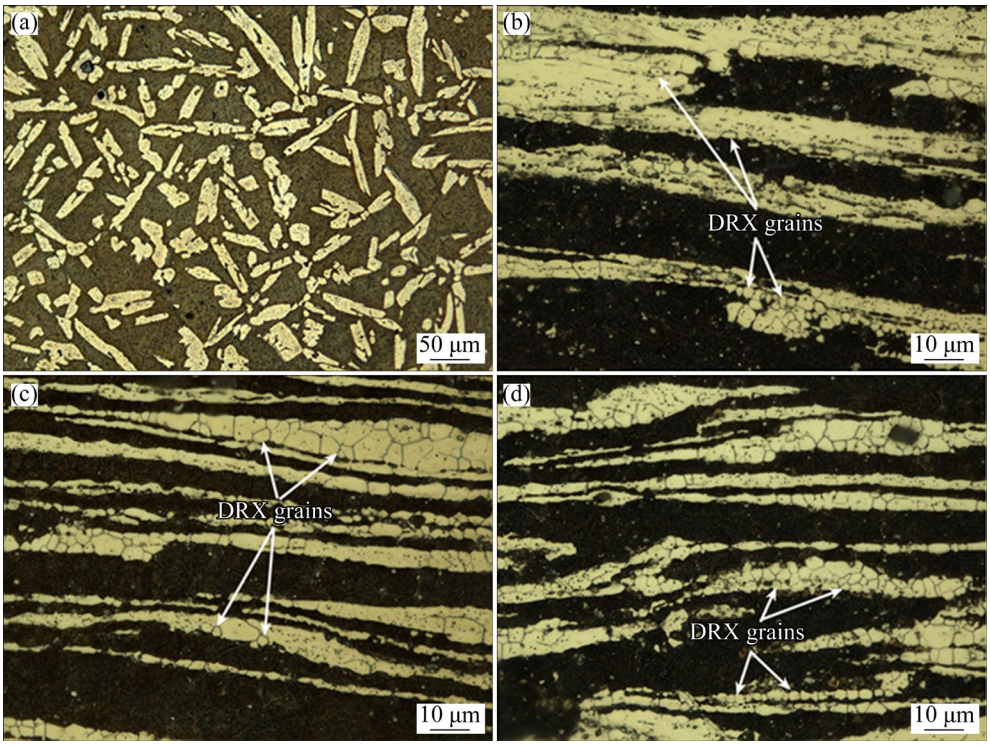

Fig. 5 OM images of as-homogenized (a) and as-extruded (b−d) Mg−8Li−6Zn−2Gd alloys with different extrusion ratios of 10:1 (b), 16:1 (c), and 23:1 (d)

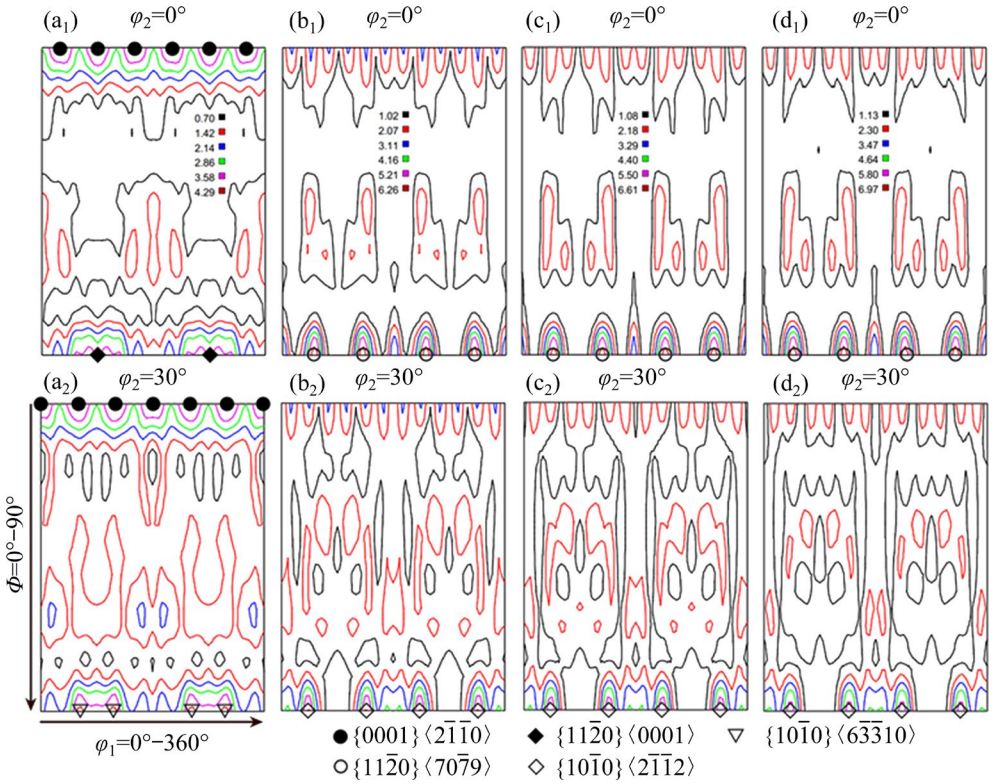

Fig. 6 ODF sections at φ_2=0° and φ_2 =30° of α-Mg phase in as-homogenized (a_1, a_2) and as-extruded (b_1−d_1, b_2−d_2) Mg−8Li−6Zn−2Gd alloys with different extrusion ratios of 10:1 (b_1, b_2), 16:1 (c_1, c_2), and 23:1 (d_1, d_2)

close to each other. After hot extrusion, the {0001}⟨2$\bar{1}\bar{1}$0⟩ basal texture weakens gradually with increasing the extrusion ratio, the {11$\bar{2}$0}⟨0001⟩ and {10$\bar{1}$0}⟨6$\bar{3}\bar{3}$10⟩ prismatic textures disappear and are replaced by the {11$\bar{2}$0}⟨70$\bar{7}$9⟩ and {10$\bar{1}$0}⟨2$\bar{1}\bar{1}$2⟩ prismatic textures. Moreover, the intensities of the {11$\bar{2}$0}⟨70$\bar{7}$9⟩ and {10$\bar{1}$0}⟨2$\bar{1}\bar{1}$2⟩ prismatic textures increase gradually with increasing extrusion ratio and are stronger than that of {0001}⟨2$\bar{1}\bar{1}$0⟩ basal texture, which might be related to the DRX behavior during hot extrusion. As some literature [21,22] suggested, the {10$\bar{1}$0} and {11$\bar{2}$0} prismatic textures result from the uniaxial deformation and DRX during extrusion process. As previously reported, texture analysis is a power means to study the plastic deformation mechanism and DRX nucleation mechanism of Mg alloys [23]. Because deformation texture is the result of the rotation and directional flow of grains during plastic deformation, recrystallization texture is caused by directional nucleation and selective growth of crystal core during recrystallization. The texture changes shown in Fig. 6 indicate that both basal slip and prismatic slip are activated during extrusion process and wherein prismatic slip contributes more to the plastic deformation. The reasons for texture evolution can be analyzed from the following aspects. Firstly, alloying Li into Mg alloy results in the increase of stacking fault energy of α-Mg matrix and the decrease in the c/a ratio of Mg lattice, which makes it easy for dislocation slip to transfer from basal plane to non-basal plane [24,25]. Additionally, the high temperature of hot extrusion can sharply reduce the critical resolved shear stress (CRSS) of prismatic slip [26]. The above reasons lead to prismatic slip becoming the main deformation mechanism of α-Mg matrix in this work, which is also the main reason why Mg−Li alloy has incomparable plastic deformation ability compared with common Mg alloy. Secondly, the addition of Zn and Gd leads to the formation of *I*-phase and *W*-phase in the alloy. They can act as recrystallization nucleation cores during hot extrusion to promote the DRX of α-Mg matrix and inhibit the growth of recrystallized grains [12,27]. This recrystallization mechanism is called particle stimulated nucleation (PSN) which can provide more nucleating approaches for DRX texture and weaken the basal texture [28]. Moreover, with

increasing the extrusion ratio (i.e. strain), more dislocations are piled up around the second phases or at the phase interfaces, and the Gibbs free energy in the alloy may increase, which supply a greater driving force for DRX [29]. Therefore, the fine recrystallized grains of α-Mg matrix increase gradually with increasing extrusion ratio. It has been reported that fine grains with a grain size smaller than 10 μm are beneficial to the activation of non-basal slip, especially prismatic slip [30,31]. According to the above analysis, the grain refinement caused by DRX also contributes to the appearance of $\{11\bar{2}0\}\langle 70\bar{7}9\rangle$ and $\{10\bar{1}0\}\langle 2\bar{1}\bar{1}2\rangle$ prismatic textures, and is the main reason for enhancement of these prismatic textures with the increase of extrusion ratio.

Figure 7 shows the orientation distribution function (ODF) sections at φ_2=0° and φ_2=45° of β-Li matrix in as-homogenized and as-extruded Mg−8Li−6Zn−2Gd alloys. There is almost no strong texture for the β-Li matrix in as-homogenized alloy, showing a random texture distribution. According to the texture distribution in Euler space for BCC metals [32−34], obvious α fiber ($\langle 110\rangle$//extrusion direction) and γ fiber ($\{111\}$//normal direction) are found on the ODF sections of β-Li matrix in as-extruded alloys. With the increase of extrusion ratio, the intensities of α fiber centered on $\{100\}\langle 110\rangle$, $\{111\}\langle 110\rangle$, $\{331\}\langle 110\rangle$ and γ fiber centered on $\{111\}\langle 110\rangle$ increase gradually. Some literature [32] suggests that α fiber and γ fiber in BCC metals are considered to be associated with recovery and recrystallization, respectively. The existence of strong α fiber means that the DRX of β-Li matrix during hot extrusion is continuous dynamic recrystallization (CDRX). Previous research has illustrated that continuous dynamic recrystallization occurs in β-Li matrix during hot extrusion below 300 °C [19]. Due to the high stacking fault energy, DRV is prone to occur in β-Li matrix. The dislocations in the original grains rearrange to form cellular structure (i.e. subgrains), and then the adjacent subgrains merge to convert low-angle grain boundaries into high-angle grain boundaries, thereby achieving the DRX nucleation of β-Li matrix. Moreover, the increase of extrusion ratio leads to more dislocations and higher Gibbs free energy, which promotes the DRV and DRX of β-Li matrix. Therefore, strong α fiber and γ fiber appear in β-Li matrix after hot extrusion and their intensities increase with increasing extrusion ratio. In addition, $\{110\}\langle 110\rangle$ texture also appears after hot extrusion and its intensity increases from 4.48 to 6.72 when the extrusion ratio increases from 10:1 to 23:1. It has been found that the $\{110\}\langle 110\rangle$ texture in BCC metals is related to DRX which appears in large shear strain zone [35].

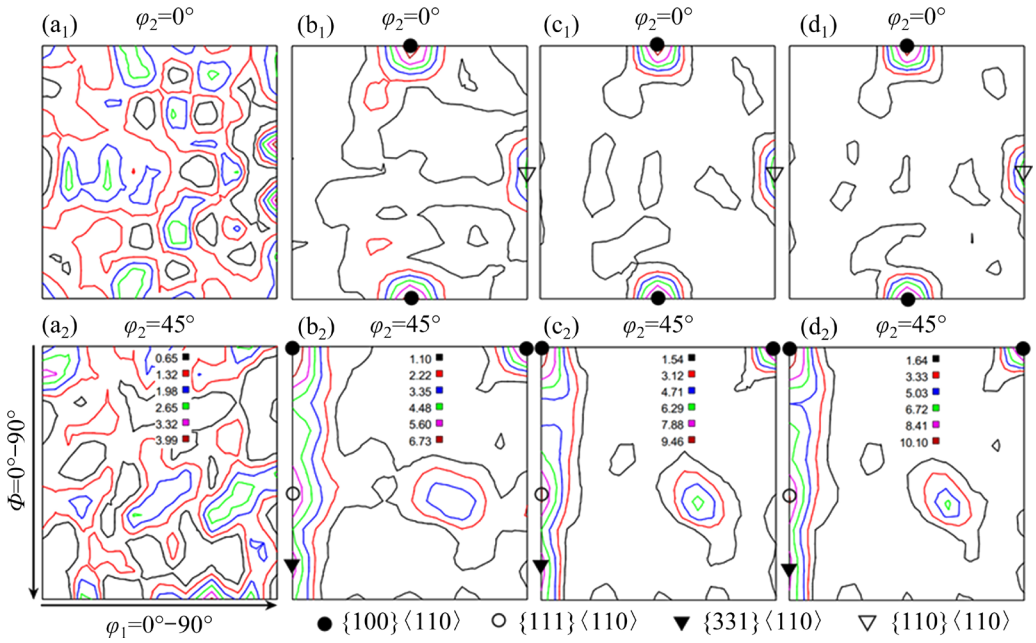

Fig. 7 ODF sections at φ_2=0° and φ_2=45° of β-Li phase in as-homogenized (a_1, a_2) and as-extruded (b_1−d_1, b_2−d_2) Mg−8Li−6Zn−2Gd alloys with different extrusion ratios of 10:1 (b_1, b_2), 16:1 (c_1, c_2), and 23:1 (d_1, d_2)

3.3 Mechanical properties

Figure 8 displays the tensile stress−strain curves of the as-homogenized and as-extruded Mg−8Li−6Zn−2Gd alloys, and the corresponding mechanical properties are listed in Table 3. The ultimate tensile strength (UTS) and elongation (δ) of the as-homogenized alloy are 185.8 MPa and 27.3%, respectively. Hot extrusion improves the tensile strength and elongation of Mg−8Li−6Zn−2Gd alloy at the same time. When the extrusion ratio increases from 10:1 to 23:1, the UTS of the alloy increases from 220.9 to 251.8 MPa, but the δ increases firstly and then decreases, and reaches the maximum of 50.6% when the extrusion ratio is 16:1. The improvement of mechanical properties is the combined result of second phase strengthening, grain refinement strengthening, and strain hardening. Firstly, many studies [8−10] have shown that introducing *I*-phase into Mg−Li alloy can significantly improve the mechanical properties of the alloy. The interface layer of α-Mg matrix within 3−5 nm in thickness maintains a coherent relationship with *I*-phase by periodically introducing ledges and steps along the interface, resulting in the rigid atomic bonding between α-Mg matrix and *I*-phase [36]. After hot extrusion, the *I*-phase in eutectic pockets is severely broken and evenly distributed in α-Mg matrix, as shown in Fig. 4. The tiny broken *I*-phase has a strong pinning effect on grain boundaries, and no cracks are observed at the α-Mg/*I*-phase interface. Therefore, the existence and fragmentation of *I*-phase are conducive to the strength and elongation of the alloy. Moreover, as extrusion ratio increases, the fragmentation degree of *I*-phase becomes severer and the size becomes smaller, so that the pinning effect on dislocations is better and the stress concentration can be reduced. However, the contribution of *W*-phase to mechanical properties is very low due to its FCC structure and incoherency between *W*-phase and alloy matrix [37]. And even it is easy to cause stress concentration around *W*-phase with a larger size during deformation, leading to microcracks and fracture. Secondly, grain refinement is considered to be the only method to simultaneously improve the strength and elongation of alloy. On the one hand, the second phases (*I*-phase and *W*-phase) in the alloy induce recrystallization nucleation and inhibit the growth of recrystallized grains, resulting in a large number of fine equiaxed recrystallized grains in the as-extruded alloys. On the other hand, the stored energy in the alloy increases with the increase of extrusion ratio, which promotes DRX. Therefore, the average grain sizes of α-Mg and β-Li in as-extruded alloys decrease with the increase of extrusion ratio, and the result is an improvement in both strength and elongation of the alloy. Thirdly, a large number of dislocations entangle and accumulate at grain boundaries and phase interfaces after hot extrusion, and the dislocation density increases with the increase of extrusion ratio, resulting in strain hardening effect. However, fully refined grains mean a decrease in the ability for grains to store dislocations during stretching, which is highly detrimental to the improvement of plasticity. At the same time, higher grain-boundary density means that more stress concentration areas exist. It has been reported that the alloys with a bimodal grain size distribution exhibit high strength and high plasticity. The high strength mainly comes from the high-density grain boundaries brought by

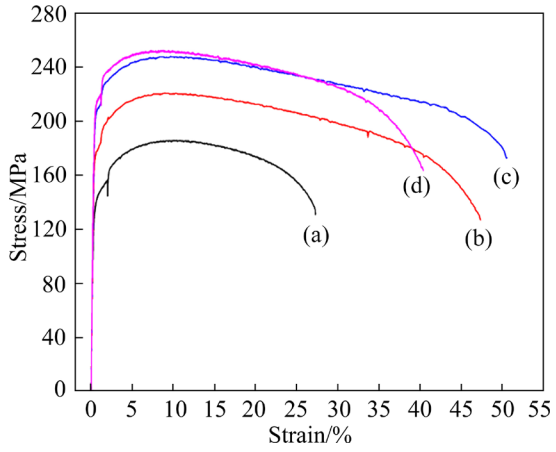

Fig. 8 Tensile stress−strain curves of as-homogenized (a) alloy and as-extruded (b−d) Mg−8Li−6Zn−2Gd alloys with different extrusion ratios of 10:1 (b), 16:1 (c), and 23:1 (d)

Table 3 Mechanical properties of as-homogenized and as-extruded Mg−8Li−6Zn−2Gd alloys

State		UTS/MPa		δ/%	
		Mean	SD[a]	Mean	SD[a]
As-homogenized		185.8	1.6	27.3	0.3
As-extruded	10:1	220.9	2.1	47.4	0.6
	16:1	248.0	2.4	50.6	0.4
	23:1	251.8	2.0	40.4	0.4

[a] SD refers to the standard deviation from the mean value

grain refinement caused by recrystallization, while high plasticity comes from the high potential for storing dislocations in the non-recrystallized grain boundary region [38,39]. Hence, strain hardening usually leads to an increase in strength and hardness but a decrease in elongation, which is also the main reason for the decrease of elongation when the extrusion ratio increases to 23:1. After hot extrusion, the strong $\{11\bar{2}0\}\langle 70\bar{7}9\rangle$ and $\{10\bar{1}0\}\langle 2\bar{1}\bar{1}2\rangle$ prismatic textures form in α-Mg matrix. These textures mean that the basal planes of most grains are not parallel or perpendicular to the extrusion direction, but have an included angle of 26.6° and 60.1° with the extrusion direction. Therefore, the texture hardening effect is very weak during the tensile testing. As the extrusion ratio increases to 16:1, the alloy exhibits a higher tensile strength of 248.0 MPa and a maximum elongation of 50.6%. After the extrusion ratio further increases to 23:1, the strength of the alloy increases only slightly, while the elongation decreases significantly. This means that for Mg−8Li−6Zn−2Gd alloy, excellent mechanical properties can be obtained by selecting an extrusion ratio of 16:1. FENG et al [40] revealed that the optimal extrusion ratio for Mg−8Li−3Al−2Zn−0.5Y alloy was also 16:1.

Figure 9 displays the fracture morphologies of as-homogenized and as-extruded Mg−8Li−6Zn−2Gd alloys. Clearly, the fracture morphologies of all alloys are full of dimples, and some broken second phases can be observed at the bottom of most dimples, exhibiting typical ductile fracture characteristic. Hot extrusion makes the dimples and the particles distributed at the bottom of dimples smaller, and the average size is the smallest when the extrusion ratio is 16:1, which are consistent with the mechanical properties shown in Fig. 8 and Table 3. The mechanism of ductile fracture in this work is microvoid coalescence fracture. During the tensile testing, many dislocations gather at the interface between second phases or matrix and α-Mg/β-Li phase interface. Due to the elastic-plastic difference and incoherency orientation relationship between matrix and second phases, many microvoids come from the rupture of second phases, the separation of second phases (W-phase and MgLiZn) from matrix, and the separation of α-Mg/β-Li phase interface. These microvoids gradually expand and

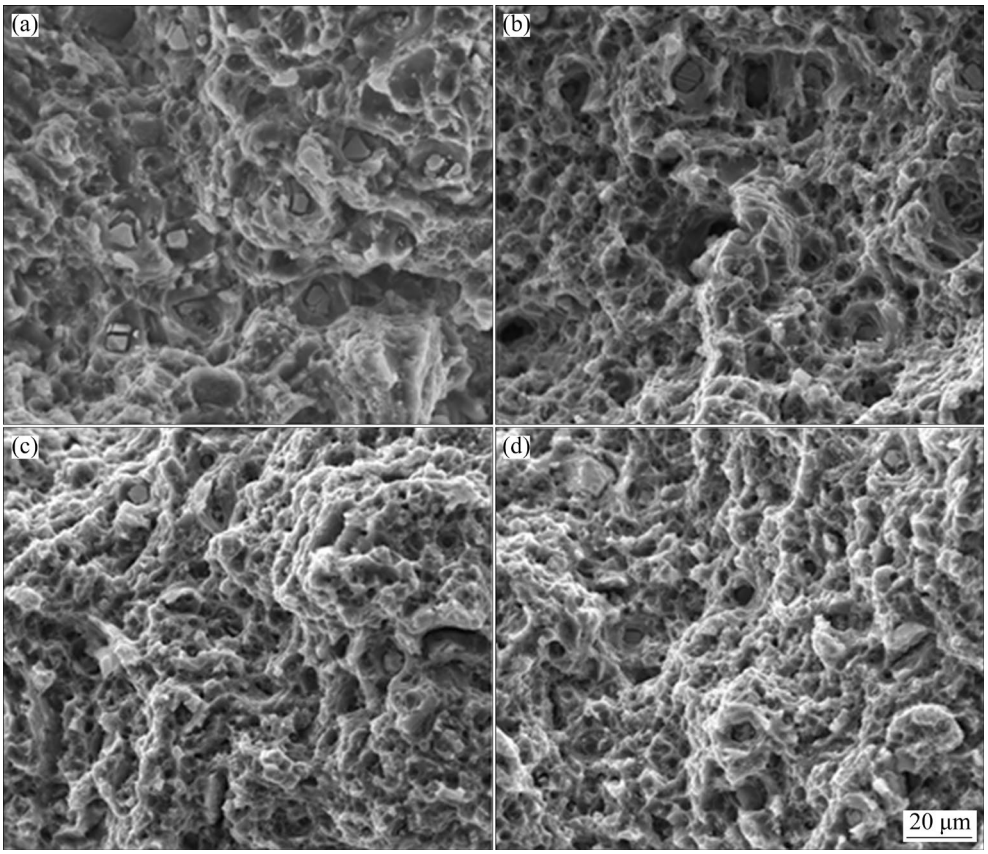

Fig. 9 Fracture morphologies of as-homogenized (a) and as-extruded (b−d) Mg−8Li−6Zn−2Gd alloys with different extrusion ratios of 10:1 (b), 16:1 (c), and 23:1 (d)

connect to each other to form microcracks, leading to the final failure fracture.

4 Conclusions

(1) The as-homogenized Mg−8Li−6Zn−2Gd alloy consists of α-Mg, β-Li, MgLiZn, *I*-phase, and *W*-phase. After hot extrusion, α-Mg and β-Li matrix phases are distributed as banded structures along extrusion direction and undergo DRX. The eutectic *I*-phase is broken into fine particles, while *W*-phase maintains massive shape but its distribution is more uniform. With increasing the extrusion ratio, the fine equiaxed grains in α-Mg and β-Li matrixes gradually increase and the grains are obviously refined.

(2) For α-Mg matrix, as the extrusion ratio increases, the $\{0001\}\langle 2\bar{1}\bar{1}0\rangle$ basal texture weakens gradually, and the $\{11\bar{2}0\}\langle 0001\rangle$ and $\{10\bar{1}0\}\langle 6\bar{3}\bar{3}10\rangle$ prismatic textures disappear. Moreover, the $\{11\bar{2}0\}\langle 70\bar{7}9\rangle$ and $\{10\bar{1}0\}\langle 2\bar{1}\bar{1}2\rangle$ prismatic textures appear and their intensities increase gradually. For β-Li matrix, α fiber, γ fiber, and $\{110\}\langle 110\rangle$ textures are observed after hot extrusion, and their intensities increase gradually with the increase of extrusion ratio.

(3) The as-homogenized Mg−8Li−6Zn−2Gd alloy has a UTS of 185.8 MPa and a δ of 27.3%. After hot extrusion, both the UTS and δ of the alloy are significantly improved, which is mainly attributed to second phase strengthening, grain refinement strengthening, and strain hardening. As the extrusion ratio increases to 16:1, the alloy exhibits the best comprehensive mechanical properties with UTS of 248 MPa and δ of 50.6%. When the extrusion ratio increases to 23:1, the UTS increases slightly, but the δ decreases significantly.

CRediT authorship contribution statement

Yue-hua SUN: Investigation, Methodology, Software, Data curation, Resources, Writing − Original draft; **Fan ZHANG:** Formal analysis, Data curation; **Bin YANG:** Formal analysis, Data curation; **Jian REN:** Investigation, Data analysis, Resources, Writing − Review & revise; **Guang-sheng SONG:** Conceptualization, Supervision.

Declaration of competing interest

The authors declare that they have no known competing financial interests or personal relationships that could have appeared to influence the work reported in this paper.

Acknowledgments

The authors are grateful for the financial supports from the Open Project of Key Laboratory of Green Fabrication and Surface Technology of Advanced Metal Materials, Ministry of Education, China (Nos. GFST2021KF04, GFST2021KF09), the Natural Science Research Project of Anhui Educational Committee, China (Nos. KJ2021A0394, KJ2021A0395), and Anhui Provincial Natural Science Foundation, China (No. 2208085QE124).

References

[1] MA Xiao-chun, JIN Si-yuan, WU Rui-zhi, WANG Jia-xiu, WANG Gui-xiang, KRIT B, BETSOFEN S. Corrosion behavior of Mg−Li alloys: A review [J]. Transactions of Nonferrous Metals Society of China, 2021, 31(11): 3228−3254.

[2] SUN Yue-hua, WANG Ri-chu, PENG Chao-qun, WANG Xiao-feng. Effect of Gd on microstructure, mechanical properties, and corrosion behavior of as-homogenized Mg−8Li−3Al−2Zn−0.2Zr alloy [J]. Transactions of Nonferrous Metals Society of China, 2022, 32(8): 2494−2509.

[3] CHAMAN-ARA M, EBRAHIMI G R, EZATPOUR H R. Deformation behavior and processing maps of Mg−Zn−Y alloy containing *I* phase at elevated temperatures [J]. Transactions of Nonferrous Metals Society of China, 2018, 28(4): 629−641.

[4] WANG Qing-feng, LIU Ke, WANG Zhao-hui, LI Shu-bo, DU Wen-bo. Microstructure, texture and mechanical properties of as-extruded Mg−Zn−Er alloys containing *W*-phase [J]. Journal of Alloys and Compounds, 2014, 602: 32−39.

[5] LIAO Hong-xin, KIM J, LEE T, SONG Jiang-feng, PENG Jian, JIANG Bin, PAN Fu-sheng. Effect of heat treatment on LPSO morphology and mechanical properties of Mg−Zn−Y−Gd alloys [J]. Journal of Magnesium and Alloys, 2020, 8: 1120−1127.

[6] LIU Yong, YUAN Guang-yin, LU Chen, DING Wen-jiang. Stable icosahedral phase in Mg−Zn−Gd alloy [J]. Scripta Materialia, 2006, 55(10): 919−922.

[7] WEI Guo-bing, PENG Xiao-dong, ZHANG Bao, HADADZADEH A, XU Tiao-cai, XIE Wei-dong. Influence of *I*-phase and *W*-phase on microstructure and mechanical properties of Mg−8Li−3Zn alloy [J]. Transactions of Nonferrous Metals Society of China, 2015, 25(3): 713−720.

[8] XU Dao-kui, LIU Lu, XU Yong-bo, HAN En-hou. The strengthening effect of icosahedral phase on as-extruded Mg−Li alloys [J]. Scripta Materialia, 2007, 57(3): 285−288.

[9] XU Dao-kui, ZU Ting-ting, YIN Min, XU Yuan-hui, HAN En-hou. Mechanical properties of the icosahedral phase reinforced duplex Mg−Li alloy both at room and elevated

temperatures [J]. Journal of Alloys and Compounds, 2014, 582: 161−166.

[10] XU Dao-kui, WANG Bao-jie, LI Chuan-qiang, ZU Ting-ting, HAN En-hou. Effect of icosahedral phase on the thermal stability and ageing response of a duplex structured Mg−Li alloy [J]. Materials & Design, 2015, 69: 124−129.

[11] LI Chuan-qiang, XU Dao-kui, YU Shuang, SHENG Li-yuan, HAN En-hou. Effect of icosahedral phase on crystallographic texture and mechanical anisotropy of Mg−4%Li based alloys [J]. Journal of Materials Science and Technology, 2017, 33(5): 475−480.

[12] LI Chuan-qiang, XU Dao-kui, WANG Bao-jie, SHENG Li-yuan, WU Rui-zhi, HAN En-hou. Effects of icosahedral phase on mechanical anisotropy of as-extruded Mg−14Li (in wt.%) based alloys [J]. Journal of Materials Science and Technology, 2019, 35(11): 2477−2484.

[13] ZHANG Yang, ZHANG Jie, WU Guo-hua, LIU Wen-cai, ZHANG Liang, DING Wen-jiang. Microstructure and tensile properties of as-extruded Mg−Li−Zn−Gd alloys reinforced with icosahedral quasicrystal phase [J]. Materials & Design, 2015, 66: 162−168.

[14] SONG Ying-wei, SHAN Da-yong, CHEN Rong-shi, HAN En-hou. Effect of second phases on the corrosion behavior of wrought Mg−Zn−Y−Zr alloy [J]. Corrosion Science, 2010, 52: 1830−1837.

[15] YAN Hong, CHEN Rong-shi, HAN En-hou. Room-temperature ductility and anisotropy of two rolled Mg−Zn−Gd alloys [J]. Materials Science and Engineering: A, 2010, 527: 3317−3322.

[16] ZHUANG Ye, ZHANG Ying-bo, ZENG Qi, LI Jia-heng. Coupling the semi-solid treatment and hot extrusion to strengthen a Mg−Zn−Gd alloy containing *I*-phase [J]. Materials Letters, 2021, 287: 129294.

[17] XU Dao-kui, HAN En-hou. Effects of icosahedral phase formation on the microstructure and mechanical improvement of Mg alloys: A review [J]. Progress in Natural Science: Materials International, 2012, 22: 364−385.

[18] GUO J, CHANG L L, ZHAO Y R, JIN Y P. Effect of Sn and Y addition on the microstructural evolution and mechanical properties of hot-extruded Mg−9Li−3Al alloy [J]. Materials Characterization, 2019, 148: 35−42.

[19] SUN Yue-hua, WANG Ri-chu, REN Jian, PENG Chao-qun, CAI Zhi-yong. Microstructure, texture, and mechanical properties of as-extruded Mg−*x*Li−3Al−2Zn−0.2Zr alloys (*x*= 5, 7, 8, 9, 11 wt.%) [J]. Materials Science and Engineering: A, 2019, 755: 201−210.

[20] LI Chuan-qiang, XU Dao-kui, WANG Bao-jie, SHENG Li-yuan, QIAO Yan-xin, HAN En-hou. Natural ageing responses of duplex structured Mg−Li based alloys [J]. Scientific Reports, 2017, 7: 40078.

[21] LASER T, HARTIG C, NÜRNBERG M R, LETZIG D, BORMANN R. The influence of calcium and cerium mischmetal on the microstructural evolution of Mg−3Al−1Zn during extrusion and resulting mechanical properties [J]. Acta Materialia, 2008, 56: 2791−2798.

[22] SHAHZAD M, WAGNER L. Influence of extrusion parameters on microstructure and texture developments, and their effects on mechanical properties of the magnesium alloy AZ80 [J]. Materials Science and Engineering: A, 2009, 506: 141−147.

[23] AGNEW S R, MEHROTRA P, LILLO T M, STOICA G M, LIAW P K. Texture evolution of five wrought magnesium alloys during route A equal channel angular extrusion: experiments and simulations [J]. Acta Materialia, 2005, 53: 3135−3146.

[24] GUO Fei, JIANG Lu-yao, MA Yan-long, LIU Lei, ZHANG Zhen, YANG Ming-bo, ZAHNG Ding-fei, PAN Fu-sheng. Strengthening a dual-phase Mg−Li alloy by strain-induced phase transformation at room temperature [J]. Scripta Materialia, 2020, 179: 16−19.

[25] LI Xiao-qiang, CHENG Chun-long, LE Qi-chi, BAO Lei, JIN Pei-peng, WANG Ping, REN Liang, WANG Hang, ZHOU Xiong, HU Cheng-lu. Investigation of Portevin-Le Chatelier effect in rolled α-phase Mg−Li alloy during tensile and compressive deformation [J]. Journal of Materials Science and Technology, 2020, 52: 152−161.

[26] CHEN Zhen-hua. Wrought magnesium alloy [M]. Beijing: Chemical Industry Press, 2005. (in Chinese)

[27] ZHOU Yu-cheng, CHEN Zhao-yun, JI Jing-han, SUN Zhi-jie. Dynamic nano precipitation behavior of as-cast Mg−4Li−4Zn−Y alloy during high temperature deformation [J]. Materials Science and Engineering: A, 2017, 707: 110−117.

[28] SUN Yue-hua, WANG Ri-chu, PENG Chao-qun, FENG Yan. Effects of Sn and Y on the microstructure, texture, and mechanical properties of as-extruded Mg−5Li−3Al−2Zn alloy [J]. Materials Science and Engineering: A, 2018, 733: 429−439.

[29] YANG Yan, PENG Xiao-dong, XIE Wei-dong, WEI Guo-bing. Influence of extrusion ratio on microstructure and mechanical behavior of Mg−9Li−3Al−2.5Sr alloy [C]//MARQUIS F. Proceedings of the 8th Pacific Rim International Congress on Advanced Materials and Processing. Cham: Springer, 2013: 1079−1089.

[30] KOIKE J. New deformation mechanisms in fine-grain Mg alloys [J]. Materials Science Forum, 2003, 419/420/421/422: 189−194.

[31] KOIKE J, KOBAYASHI T, MUKAI T, WATANABE H, SUZUKI M, MARUYAMA K, HIGASHI K. The activity of non-basal slip systems and dynamic recovery at room temperature in fine-grained AZ31B magnesium alloys [J]. Acta Materialia, 2003, 51: 2055−2065.

[32] ZOU Yun, ZHANG Le-hao, WANG Hong-tao, TONG Xin, ZHANG Mi-lin, ZHANG Zhong-wu. Texture evolution and their effects on the mechanical properties of duplex Mg−Li alloy [J]. Journal of Alloys and Compounds, 2016, 669: 72−78.

[33] SHEN G J, DUGGAN B J. Texture development in a cold-rolled and annealed body-centered-cubic Mg−Li alloy [J]. Metallurgical and Materials Transactions A, 2007, 38: 2593−2601.

[34] PARK Y B, LEE D N, GOTTSTEIN G. The evolution of recrystallization textures in body centred cubic metals [J]. Acta Materialia, 1998, 46: 3371−3379.

[35] LIU Yan-dong, JIANG Qi-wu, WANG Gang, WANG Yan-dong, TIDU A, ZOU Liang. Influence of microstructures and textures on the torsional behavior of pearlitic wires [J]. Journal of Materials Science and Technology, 2005, 21:

357−360.
[36] BAE D H, KIM S H, KIM D H, KIM W T. Deformation behavior of Mg−Zn−Y alloys reinforced by icosahedral quasicrystalline particles [J]. Acta Materialia, 2002, 50: 2343−2356.
[37] XU Dao-kui, LIU Lu, XU Yong-bo, HAN En-hou. The influence of element Y on the mechanical properties of the as-extruded Mg−Zn−Y−Zr alloys [J]. Journal of Alloys and Compounds, 2006, 426: 155−161.
[38] WITKIN D, LEE Z, RODRIGUEZ R, NUTT S, LAVERNIA E. Al−Mg alloy engineered with bimodal grain size for high strength and increased ductility [J]. Scripta Materialia, 2003, 49(4): 297−302.
[39] KIM Y J, LEE J U, KIM S H, KIM Y M, PARK S H. Grain size effect on twinning and annealing behaviors of rolled magnesium alloy with bimodal structure [J]. Materials Science and Engineering: A, 2019, 754: 38−45.
[40] FENG Shi, LIU Wen-cai, ZHAO Jiong, WU Guo-hua, ZHANG Hao-hao, DING Wen-jiang. Effect of extrusion ratio on microstructure and mechanical properties of Mg−8Li−3Al−2Zn−0.5Y alloy with duplex structure [J]. Materials Science and Engineering: A, 2017, 692: 9−16.

挤压比对双相 Mg−8Li−6Zn−2Gd 合金显微组织、织构和力学性能的影响

孙月花[1,2]，张 帆[2]，杨 滨[2]，任 建[1,2]，宋广生[1,2]

1. 安徽工业大学 先进金属材料绿色制备与表面技术教育部重点实验室，马鞍山 243002
2. 安徽工业大学 材料科学与工程学院，马鞍山 243002

摘 要：通过显微组织观察、织构分析和拉伸测试等手段研究挤压比对双相 Mg−8Li−6Zn−2Gd 合金显微组织、织构和力学性能的影响。结果表明：均匀化态 Mg−8Li−6Zn−2Gd 合金中含有 α-Mg、β-Li、MgLiZn、*I* 相和 *W* 相。经热挤压后，共晶 *I* 相被碾碎成细小颗粒状，而 *W* 相保持原有块状形状。合金中 α-Mg 基体和 β-Li 基体在热挤压过程中均发生了动态再结晶(DRX)，且晶粒随着挤压比的增加逐渐细化。经热挤压后，α-Mg 基体的基面织构弱化和柱面织构增强是由于非基面滑移的激活；β-Li 基体中形成明显的 α 和 γ 纤维织构主要与动态回复与动态再结晶相关。热挤压同时提升 Mg−8Li−6Zn−2Gd 合金的抗拉强度和伸长率，并在挤压比为 16:1 时获得最佳的综合力学性能。

关键词：Mg−Li 合金；二十面体准晶相；挤压比；动态再结晶；宏观织构；力学性能

(Edited by Wei-ping CHEN)